JGR Planets

RESEARCH ARTICLE

10.1029/2025JE009316

Strong Variability of the Modeled Venus NO Nightglow

N. Streel[1,2], F. Lefèvre[1], A. Martinez[3], A. Määttänen[1], A. Stolzenbach[3], S. Lebonnois[4], J. C. Gérard[5], and L. Soret[5]

[1]LATMOS/IPSL, Sorbonne Université, UVSQ Université Paris-Saclay, CNRS, Paris, France, [2]Planetary Atmospheres Group, Institute for Basic Science (IBS), Daejeon, South Korea, [3]Instituto de Astrofísica de Andalucía (IAA-CSIC), Granada, Spain, [4]LMD Sorbonne Université, ENS, Ecole Polytechnique, CNRS, Paris, France, [5]LPAP-STAR, Université de Liège, Liège, Belgium

Abstract The ultraviolet nightglow of nitric oxide (NO) on Venus offers a unique window into the dynamics and chemistry of its upper atmosphere. We present three-dimensional simulations of Venus' NO nightglow using a ground-to-thermosphere model, revealing a strong, short-timescale variability consistent with observations. The Venus Planetary Climate Model accurately reproduces the altitude of peak emission at 115 km, matching SPICAV data, and shows an average peak brightness of 53 ± 33 kR, only 5% below the observed values. Crucially, the observed variability and morphology of the NO emission are tightly linked to atmospheric dynamics; its maxima strongly correlate with horizontal wind convergence, leading to localized subsidence. This downward transport is essential for delivering nitrogen atoms to fuel the nightglow, making it a critical tracer for understanding Venus's complex atmospheric circulation. Our findings underscore the importance of the NO nightglow as a powerful diagnostic for the solar-to-antisolar circulation on Venus.

Plain Language Summary The faint ultraviolet glow (nightglow) of nitric oxide (NO) on Venus is a key indicator of gas movements in its upper atmosphere. Our advanced computer model of the Venusian atmosphere, extending from the surface to the upper atmosphere, reproduces this glow and its strong and rapid variations. We show that the NO glow is bright and located at an altitude of 115 km, which matches observations from past satellite missions. The brightest areas of the NO nightglow are strongly linked to the convergence of horizontal winds, which causes the air to descend. This movement is crucial as it brings the nitrogen and oxygen necessary for the formation of the emission. Thus, the significant changes in the NO nightglow directly reflect the complex and variable patterns of Venus's atmospheric winds, making this glow a powerful tool for studying Venusian atmospheric circulation.

Key Points:

- A global climate model of Venus simulates complex, filamentary NO nightglow morphology
- The model successfully reproduces the observed strong short-timescale variability of the NO nightglow
- The NO nightglow variability is strongly linked to localized convergence and subsidence at 115 km altitude

Supporting Information:

Supporting Information may be found in the online version of this article.

Correspondence to:

N. Streel,
Nicolas.streel@latmos.ipsl.fr

Citation:

Streel, N., Lefèvre, F., Martinez, A., Määttänen, A., Stolzenbach, A., Lebonnois, S., et al. (2026). Strong variability of the modeled Venus NO nightglow. *Journal of Geophysical Research: Planets*, *131*, e2025JE009316. https://doi.org/10.1029/2025JE009316

Received 10 JUL 2025
Accepted 1 APR 2026

1. Introduction

On Venus, the nitric oxide nightglow is an ultraviolet emission that is generated as follows: on the dayside hemisphere, CO_2 and N_2 are photodissociated by extreme ultraviolet (EUV) photons and photoelectrons. These processes create oxygen and nitrogen atoms in their ground states O(^{3}P) and N(^{4}S), which are then transported to the nightside by the subsolar-to-antisolar circulation (SS-AS). On the nightside, oxygen and nitrogen atoms are transported downwards, where recombination takes place and produces NO molecules in the $\left(C^2\Pi\right)$ electronic state:

$$N + O \rightarrow \mathrm{NO}\left(C^2\Pi\right)$$

The relaxation of those excited NO molecules toward the $\left(X^2\Pi\right)$ electronic state generates the emission of ultraviolet photons in two bands, δ (190–240 nm) and γ (225–270 nm) (Feldman et al., 1979):

$$\mathrm{NO}\left(C^2\Pi\right) \rightarrow \mathrm{NO}\left(X^2\Pi\right) + \delta \text{ bands}$$

$$NO\left(C^2\Pi\right) \rightarrow NO\left(A^2\Sigma, v' = 0\right) + 1.22\ \mu\mathrm{m}$$

$$\mathrm{NO}\left(A^2\Sigma, v' = 0\right) \rightarrow NO\left(X^2\Pi\right) + \gamma \text{ bands}$$

The total emission rate of NO is proportional to the N and O number densities, which makes the NO nightglow a valuable tracer of the dynamics, temperature and chemistry of the upper atmosphere. The NO nightglow on Venus

was first detected and identified by Feldman et al. (1979) using an ultraviolet spectrograph on board the International Ultraviolet Explorer. In the same year, the NO nightglow was also detected by the ultraviolet spectrometer instrument on Pioneer Venus Orbiter (OUVS, Stewart et al., 1980), providing the first map of the emission. More recently, the Venus Express mission (2006–2014) provided an extensive set of nightglow data from the SPICAV ultraviolet spectrometer in various observation modes (Gérard et al., 2008; Royer et al., 2010; Stiepen et al., 2012, 2013).

The peak of the NO nightglow is usually found between 105 and 120 km, with 115 km as the average peak altitude (Gérard et al., 1981, 2008; Royer et al., 2010, 2016; Stiepen et al., 2013). This altitude range is located in a layer of transition between the SS-AS circulation above 120 km, and the retrograde zonal super-rotation that is dominant below ∼70 km. As a result of this dynamical complexity, the NO emission is typically brightest in a wide region centered at about 02:00 local time (LT) and distributed over a wide range of latitudes over the equator (Gérard et al., 2008; Stewart et al., 1980; Stiepen et al., 2013). The nightglow also presents a strong short-term variability (Royer et al., 2010) characterized by sudden changes in the distribution with timescales of a few Earth days and a patchy distribution. The integrated emission measured in kilo-Rayleigh (kR, where 1 kR = $10^{13}/(4\pi)$ photon m^{-2} sr^{-1} s^{-1}) shows a hemispheric mean of about 2 kR (Bougher et al., 1990; Stiepen et al., 2013).

Most of the simulations of the NO nightglow on Venus were performed with one-dimensional (e.g., Gérard et al., 2008; Krasnopolsky, 2010) or two-dimensional (Collet et al., 2010) models. These tools provide a good approximation of the mean profile of the NO emission but, by nature, can reproduce neither the three-dimensional complexity of the dynamics involved in the NO nightglow nor its spatial and temporal variability. The situation was greatly improved by the three-dimensional simulations of the NO nightglow by the Venus Thermospheric General Circulation Model (VTGCM, Bougher et al., 1990; Brecht et al., 2011). Using sensitivity tests on different key parameters, studies with the VTGCM enabled a precise examination of the mechanisms underlying the NO emission and its shift toward the morning side. However, only a few observations of SPICAV were available at that time. The comparison with the VTGCM was therefore limited to 17 orbits and 201 limb scans between 2005 and 2008, making the investigation of the NO nightglow variability difficult.

This paper aims to advance our quantitative understanding of the NO nightglow on Venus, using the full extent (2006–2011) of the published SPICAV data set and a state-of-the-art general circulation model with photochemistry. The SPICAV measurements constitute by far the largest observational database concerning the NO nightglow on Venus. These nadir and limb observations document the distribution of the column-integrated nightglow both in latitude and local time when viewed from the nadir (Stiepen et al., 2013), and its vertical profile in limb viewing (Stiepen et al., 2012). In addition, over the long period of the Venus Express mission, the SPICAV instrument has provided unique insight into the variability of the NO nightglow (e.g., Royer et al., 2010). We compare here the full set of the SPICAV data to the NO nightglow calculated by our model and analyze the processes at the origin of the nightglow variability.

2. The Venus Planetary Climate Model

The Venus Planetary Climate Model (Venus PCM), formerly known as the IPSL Venus Global Climate Model, was first described in Lebonnois et al. (2010). This model includes full physics, with a radiative transfer that accounts for solar heating rates (Crisp, 1986), infrared net exchange rates (Eymet et al., 2009), specific heat changes with temperature (Lebonnois et al., 2010), Magellan topography (Ford & Pettengill, 1992), and coupled photochemistry (Stolzenbach et al., 2023). We use the 90-level configuration of the Venus PCM, extending up to approximately 250 km in the thermosphere (Martinez et al., 2023). This version includes parameterizations of CO_2-O cooling, non-LTE CO_2 heating, thermal conduction, molecular viscosity, extreme ultraviolet heating, and non-orographic gravity waves (Gilli et al., 2017, 2021). Charged species are also implemented to represent the ionosphere (Martinez et al., 2024). Compared to the simulations presented by Stolzenbach et al. (2023), the horizontal resolution of the simulations presented here is more than doubled from 7.5° × 5.625° to 3.75° × 1.875° (96 longitudes × 96 latitudes). We also modified the eddy diffusion coefficient used in the upper atmosphere, which is now defined as $K = A\sqrt{n}$ with units of cm^2 s^{-1}, where n is the total number density in cm^{-3} and $A = 5.5 \times 10^{12}$ $cm^{0.5}$ s^{-1} (Bougher et al., 2015; Von Zahn et al., 1980). The upper limit of K was set to 200 cm^2 s^{-1}.

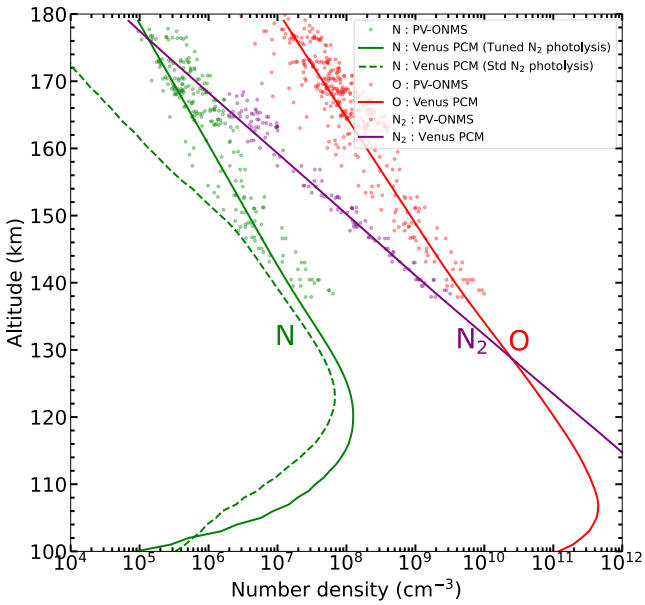

Figure 1. Vertical distribution of N, N2, and O on the nightside (02:00–03:00 LT) of Venus. Circles: observations from the Pioneer Venus ONMS mass spectrometer (Kasprzak et al., 1993; Niemann et al., 1980). Dotted: Venus PCM with standard N_2 photolysis. Solid: Venus PCM with doubled N_2 photolysis.

For the NO nightglow simulations conducted here, we brought several improvements to the photochemical module of the Venus PCM, briefly described below.

2.1. On-Line Photolysis

In the original version of the Venus PCM with photochemistry, as described by Stolzenbach et al. (2023), photolysis rates were calculated offline and stored in a lookup table that was a function of the CO_2 column, SO_2 column, and solar zenith angle. In the improved code used here, photolysis rates are calculated online, following the same strategy as in the Mars version of the PCM (Lefèvre et al., 2021). This update incorporates the screening effect of all ultraviolet-absorbing species in the computation of the photolysis rates and improves the accounting of local effects of temperature or cloud opacity. The radiative transfer computation is performed over the range of 0–815 nm in 194 spectral bins, with a variable resolution adapted to resolve the Lyman-alpha line (0.2 nm) and the fine structures of the CO_2 and SO_2 absorption cross-sections (0.5–1.0 nm). The solar flux used was representative of average activity conditions (140 s.f.u.)

2.2. Nitrogen Photochemistry

The photochemical module described in Stolzenbach et al. (2023) includes the chemistry of CO_2, CO, hydrogen, oxygen, chlorine and sulfur. To study the NO nightglow, we have added the description of N, N(^{2}D), NO, and NO_2, leading to a total of 40 chemical species in the model. The new photolytic, chemical, and ionic reactions related to nitrogen are listed in Table S1 of Supporting Information S1.

Reactive nitrogen primarily originates from the photodissociation of N_2 at altitudes above 140 km. For an accurate computation of the production of N atoms, ultra-high spectral resolution is required in the highly structured regions of the N_2 absorption cross-section. Computations carried out at low spectral resolution in photochemical models, such as those made in the Venus PCM, are therefore recognized to be largely uncertain. Furthermore, information regarding the branching ratios to the various possible channels throughout the entire range of photodissociation is currently unavailable (Fox et al., 2008). To alleviate these problems, we have chosen to constrain the photolysis of N_2 based on the N atom profile measured by the Neutral Mass Spectrometer on board Pioneer Venus Orbiter (ONMS; Niemann et al., 1980; Kasprzak et al., 1993). Figure 1 compares the vertical distribution of N between 140 and 180 km measured by ONMS and calculated by the Venus PCM. In its standard version, the model significantly underestimates the number of N atoms, whereas the N_2 profile agrees with the observations. This indicates that the model bias is due to the lack of spectral resolution in calculating N_2 photolysis (and the uncertainties on the branching ratios mentioned above) rather than an underestimate of N_2 number density. To ensure that the production of reactive nitrogen is in line with the observations, we adjusted the N_2 photolysis rate to obtain a N profile that matches the ONMS observations. In practice, multiplying the N_2 photolysis rate by a factor of two is sufficient for the amount of N produced by the model to match that measured by ONMS on the nightside, where the NO emission occurs (Figure 1). This scaling is comparable to the threefold factor Brecht et al., 2011 applied to the VTGCM for the same reasons. With this correction, applied to the simulations presented in the rest of the paper, the nightside density profile of N peaks at 1.5×10^8 cm^{-3} at 115 km. This value is in good agreement with the N number density of 1.4×10^8 cm^{-3} calculated at 115 km with the VTGCM by Brecht et al. (2011). Regarding atomic oxygen O, the other precursor of NO, Figure 1 shows that the model is in line with the vertical profile retrieved from ONMS down to 140 km (Kasprzak et al., 1993). The O peak occurs at 107 km, close to the altitude of 103–106 km determined experimentally from the VIRTIS instrument (Soret et al., 2012). The O number density at the peak is overestimated by about a factor of 2.5 (4.7×10^{11} cm^{-3} vs. 1.9×10^{11} cm^{-3}) relative to VIRTIS. However, the number density of NO is primarily restricted by that of N, which is considerably lower—three orders of magnitude—than that of O. The NO nightglow is therefore weakly sensitive to the precise quantity of O calculated by the model.

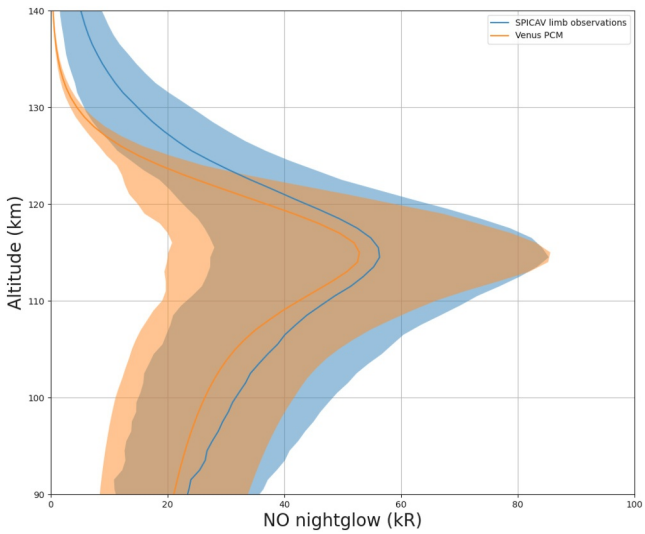

Figure 2. Vertical distribution of the NO nightglow (kR) observed by SPICAV (blue) and calculated by the Venus PCM (orange). SPICAV data have been averaged over all limb observations (2006–2011) presented by Stiepen et al. (2012). Venus PCM nightglow is an average of all model profiles co-located with SPICAV observations. Shading represents one-sigma variability.

3. SPICAV Observations

The SPICAV instrument (Bertaux et al., 2007) is a suite of three spectrometers aboard the Venus Express spacecraft that flew from 2006 to 2014. The ultraviolet spectrometer covered the 118–320 nm region and could simultaneously observe both the δ and γ bands of the NO nightglow. During its mission, SPICAV detected the NO nightglow in two different observation geometries: in limb-viewing, Stiepen et al. (2012) retrieved the vertical profile of the NO nightglow with a typical error of about 10%. The NO data set is based on 98 orbits and 865 individual limb scans conducted between 2006 and 2011. Because of the near-polar elliptical orbit of Venus Express, limb measurements were preferentially taken when SPICAV was observing the northern hemisphere and covered the local times between 06:00 LT and 18:00 LT. In nadir viewing, Stiepen et al. (2013) derived a statistical distribution of the vertically integrated NO nightglow measured during 1,600 orbits between 2006 and 2011. The NO emission map is binned onto a 5° latitude × 5° longitude grid, equivalent to a 20-min resolution in local time. However, due to the characteristics of the orbit and the fact that nadir observations were performed only when the spacecraft was entirely within the Venus eclipse, there is a distinct inhomogeneity in the geographical distribution of the SPICAV data. The regions north of 60°S and south of 40°S were practically unobserved (Stiepen et al., 2013).

4. Modeling the NO Nightglow

4.1. Comparison With SPICAV Limb and Nadir Data

We first examine the vertical distribution of the NO emission as observed at the limb by SPICAV and calculated by the Venus PCM. The mean SPICAV profile, shown in blue in Figure 2, is obtained by summing all profiles collected between 2006 and 2011, after deconvolution of the instrument's point spread function and rejection of profiles showing no unambiguous NO emission (Stiepen et al., 2012). The observed NO nightglow exhibits a mean altitude of the emission peak at approximately 115 km, consistent with prior satellite observations (Gérard et al., 1981, 2008; Royer et al., 2010). The mean intensity at the peak was 56 kR. A striking feature of the SPICAV observations is the significant variability in the NO nightglow at all altitudes. The brightness is quite variable with a one-sigma standard deviation of 29 kR (∼50%) at the emission peak.

The Venus PCM results have been directly compared to the limb emissions observed by SPICAV, without the need to invert the local volume emission rate from the observations. For each limb scan, the NO nightglow calculated by the model has been integrated along the simulated line of sight, assuming spherical symmetry of the emission rate. The obtained NO nightglow profile, averaged over all SPICAV observations, is presented in Figure 2. The altitude of the peak emission modeled by the Venus PCM, located at 115 km, is in excellent agreement with SPICAV. The average brightness at the peak is 53 ± 33 kR, only 5% less than the observed value. Similarly to SPICAV, the model also shows a strong variability of the NO nightglow, with a one-sigma standard deviation of the order of 50% and a maximum emission of 85 kR at 155 km. Above the emission peak, the nightglow profile observed by SPICAV in Figure 2 decreases less steeply with altitude than that calculated by the Venus PCM. This contrasts with the modeled NO emission, which converges rapidly toward zero from 130 km upwards, in agreement with other one-dimensional (Krasnopolsky, 2013; Stiepen et al., 2012) and three-dimensional (Brecht et al., 2011) models. The fact that the topside SPICAV airglow decreases with a significantly larger apparent scale height than expected from PV-OUVS (Gérard et al., 1981) of the theory is discussed in detail by Gérard et al. (2008). This effect results essentially from the size of the SPICAV field of view on the limb (between 3 and 27 km), which tends to smooth the observed limb profile and increase the apparent topside scale height. Therefore, the difference between the Venus PCM and SPICAV above 125 km can be attributed to observational effects and does not necessarily reflect an underestimation of the NO nightglow by the model.

We now consider the observations of the NO nightglow performed by the SPICAV instrument in the nadir mode. Figure 3a presents the nightglow map constructed by Stiepen et al. (2013) from the data set obtained between

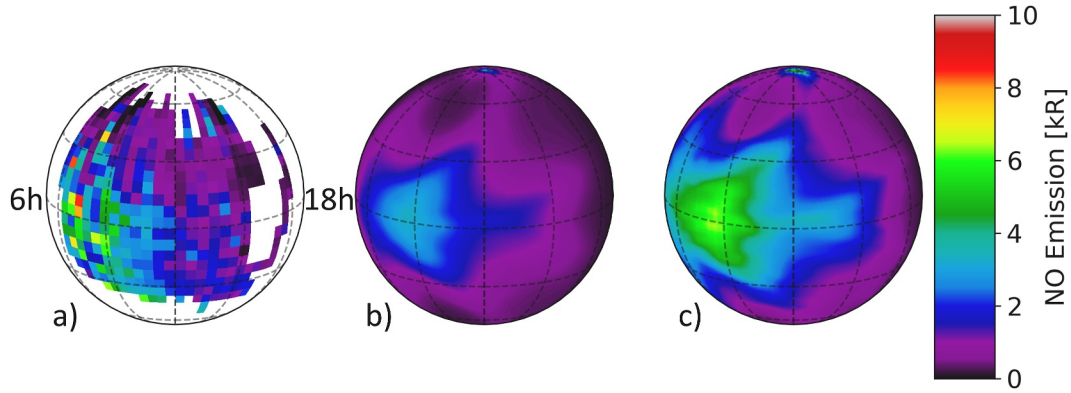

Figure 3. Column-integrated NO nightglow (kR) on Venus. Left: (a) SPICAV nadir observations (Stiepen et al., 2013). The data are averaged over 6 years of measurements. Areas without observations are depicted in white. Middle: (b) Modelled NO nightglow, average over one Venus day (116.75 Earth days). Right: (c) modeled NO nightglow, upper 2-sigma limit over one Venus day. Maps are centered at midnight (anti-solar point).

2006 and 2011. The region of enhanced NO emission is shifted toward the morning side of the nighttime hemisphere, extending between local times 01:00 and 03:30 LT and latitudes 25°S to 10°N. The typical uncertainty ranges from 0.1 to 0.8 kR. As discussed by Stiepen et al. (2013), the coverage of the SPICAV data in nadir mode is highly non-uniform and distributed very unevenly over time. In particular, the SPICAV observation time for the brightest region of emission was short compared with that for the rest of the observed areas. This results in poorer statistics and may explain the patchy character of the brightest nightglow area, which shows a high degree of variability on adjacent pixels.

To compare our model with the SPICAV data in nadir mode, we vertically integrated the NO emission calculated by the Venus PCM and averaged it over one Venus day (116.75 Earth days). The result is mapped in Figure 3b. The modeled NO nightglow shows a distinct maximum located on the morning side of the Venus disk. The brightest region extends from 22:00 LT to 04:00 LT, in good agreement with the OUVS and SPICAV observations. Its latitudinal extent is fairly symmetric between both hemispheres, but is smaller than that observed by SPICAV.

In quantitative terms, the mean intensity averaged over one Venus day by the Venus PCM is generally lower than that indicated in the SPICAV map. The mean intensity modeled in the brightest region is about 3 kR, compared with 3.9 kR measured by SPICAV. When averaged over the same spatial domain as the SPICAV data, the hemispheric mean of the NO brightness predicted by the Venus PCM is 1.1 kR, about 40% lower than the observed value of 1.9 kR (Stiepen et al., 2013). However, as with the limb profiles presented previously, the model shows strong day-to-day variability in NO brightness. Over one Venus day, Figure 3c shows values of the upper 2-sigma bound that are twice as high and largely consistent with the SPICAV measurements.

Stewart and Barth (1979) first reported the day-to-day variability of NO nightglow emission by comparing images taken 24 hr apart by the Pioneer Venus OUVS spectrometer. Stewart et al. (1980) and Bougher et al. (1990) continued this study with an extended OUVS data set and described bright patches appearing randomly at various latitudes and local times. This large variability of the NO nightglow was also found by Gérard et al. (2008) from an early set of the SPICAV limb observations, and by Royer et al. (2010) from the SPICAV data in stellar occultation mode. Localized regions of enhanced or decreased downward fluxes of atoms have been proposed to explain the patchy structure observed on the individual maps of NO nightglow.

Examining the instantaneous nightglow maps calculated by the model enables visualization of the typical morphology and short-timescale variability of the NO emission. The example in Figure 4 illustrates a complex structure, characterized by elongated features that can extend both zonally and meridionally. These maps reveal a pronounced spatial variability, a critical observation given that they are separated by roughly one Earth day (1/100th of a Venusian day). Since the morphology of the NO emission changes rapidly from one Earth day to the next, a region of strong NO brightness may be devoid of any emission the next day, and vice versa. This result explains the strong variability evident in the nightglow NO measurements, whether taken in nadir mode

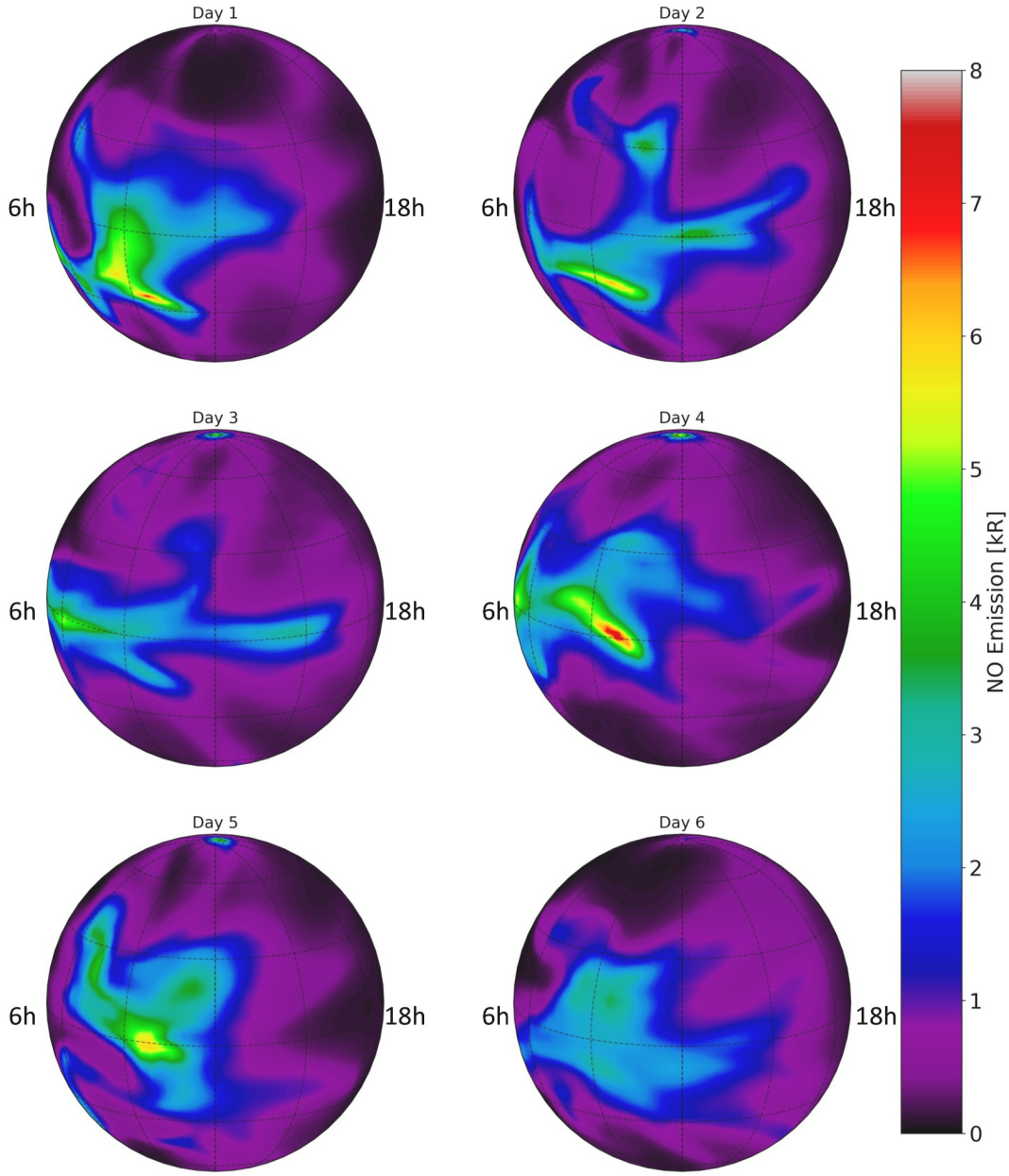

Figure 4. Instantaneous column-integrated NO nightglow (kR) calculated by the Venus PCM over six consecutive Earth days. The maps are centered at midnight (anti-solar point) and are separated by one Earth day.

(e.g., Bougher et al., 1990; Stewart et al., 1980; Stiepen et al., 2013) or while viewing the limb (Royer et al., 2010; Stiepen et al., 2012). Both the morphology and the variability of the NO nightglow simulated by the Venus PCM are reminiscent of those of the $O_2(^1\Delta)$ nightglow, as suggested by Gérard et al. (2017) and calculated with the same model by Navarro et al. (2021). The NO and $O_2(^1\Delta)$ nightglows are subject to the same complex variable dynamics of the SS-AS circulation.

In quantitative terms, Figure 4 shows that the value of maximum brightness can easily vary by a factor of 2 from one Earth day to the next, and can be located in a very different region, sometimes quite far from the equator (−25°S). We note that brightnesses above 7 kR can be reached locally, which approaches the few most intense pixels detected by SPICAV (Figure 3a). Secondary maxima are also present in the modeled nightglow maps, at latitudes sometimes reaching 30°N and local times as early as 22:00 LT. In the example of the 6 Earth days selected in Figure 4, significant NO emission can occur in long filaments stretching up to 50°N or S. All these

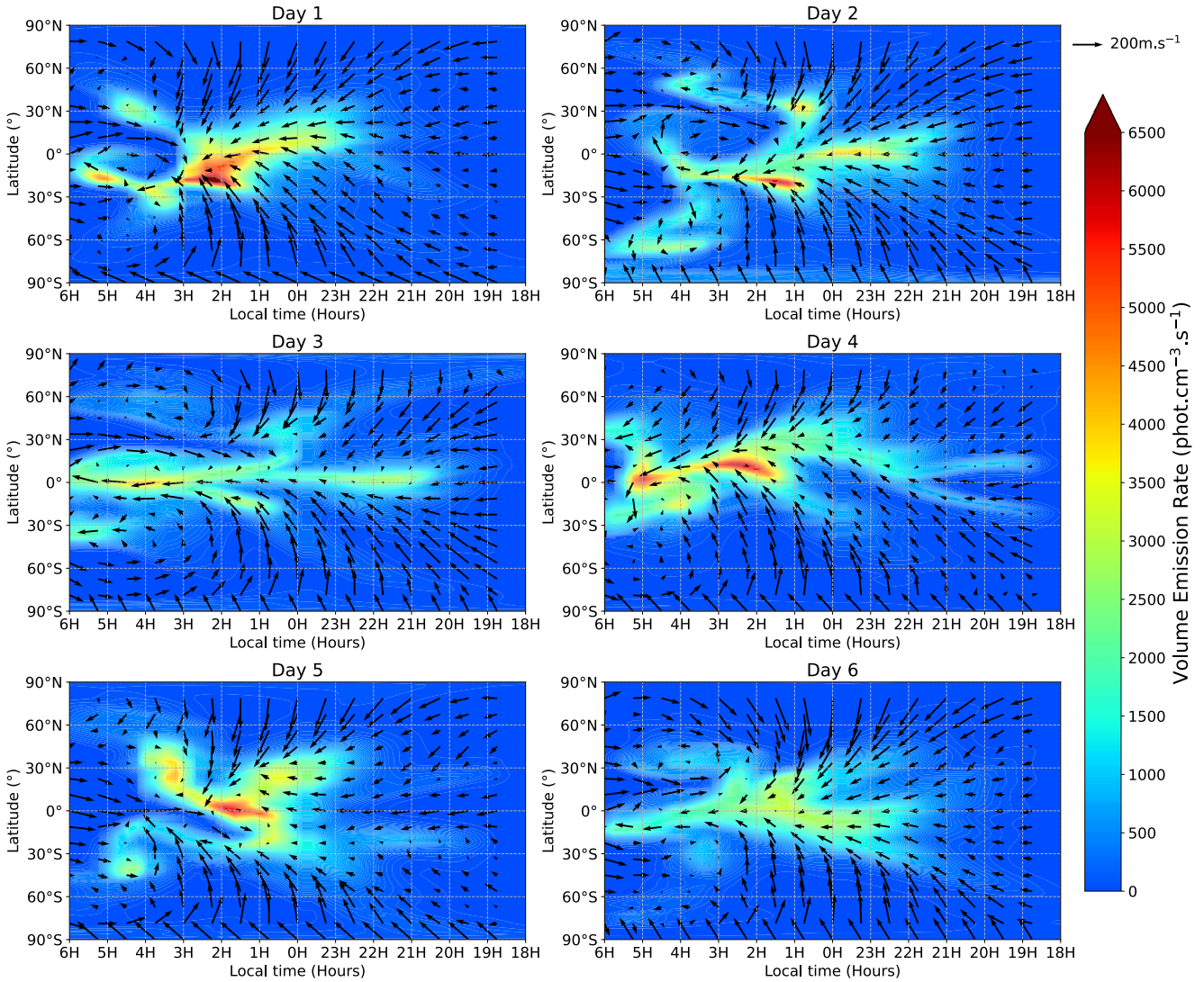

Figure 5. Instantaneous NO nightglow (photon cm^{-3} s^{-1}) and horizontal wind (m s^{-1}) calculated at 115 km by the Venus PCM over the six consecutive Earth days considered in Figure 4.

features are consistent with the variability of the OUVS data reported by Bougher et al. (1990). In summary, the canonical picture of a steady, broad maximum centered on the equator at 02:00 LT does not reflect the reality of the NO nightglow distribution on Venus. This conclusion was already reached by Soret et al. (2014) for the $O_2(^1\Delta)$ Venus nightglow. Although this view remains accurate from a time-averaged perspective, as shown in Figure 3, it is likely that the morphology of the region of NO emission at any given time never looks like this. Our simulations indicate, on the contrary, that the NO nightglow region exhibits a complex and highly variable shape, with its contours changing daily. As it frequently extends in long filaments to high latitudes, or even toward the evening terminator, the NO emission can occur in almost any region of the Venus nightside.

4.2. Analyzing Nightglow Variability

The characteristics of the NO nightglow described above are now compared to those of the horizontal and vertical winds calculated by the Venus PCM. Figure 5 superimposes the nightglow calculated at the emission peak, around 115 km, on the horizontal wind field calculated by the Venus PCM. At this discrete altitude level, the filamentary nature of the NO emission region is even more evident than in the vertically integrated brightness maps (Figure 4). Over the 6 Earth days considered here, the region of strongest nightglow is strongly correlated with a maximum convergence of the SS-AS circulation on the horizontal plane. On average, this region is located

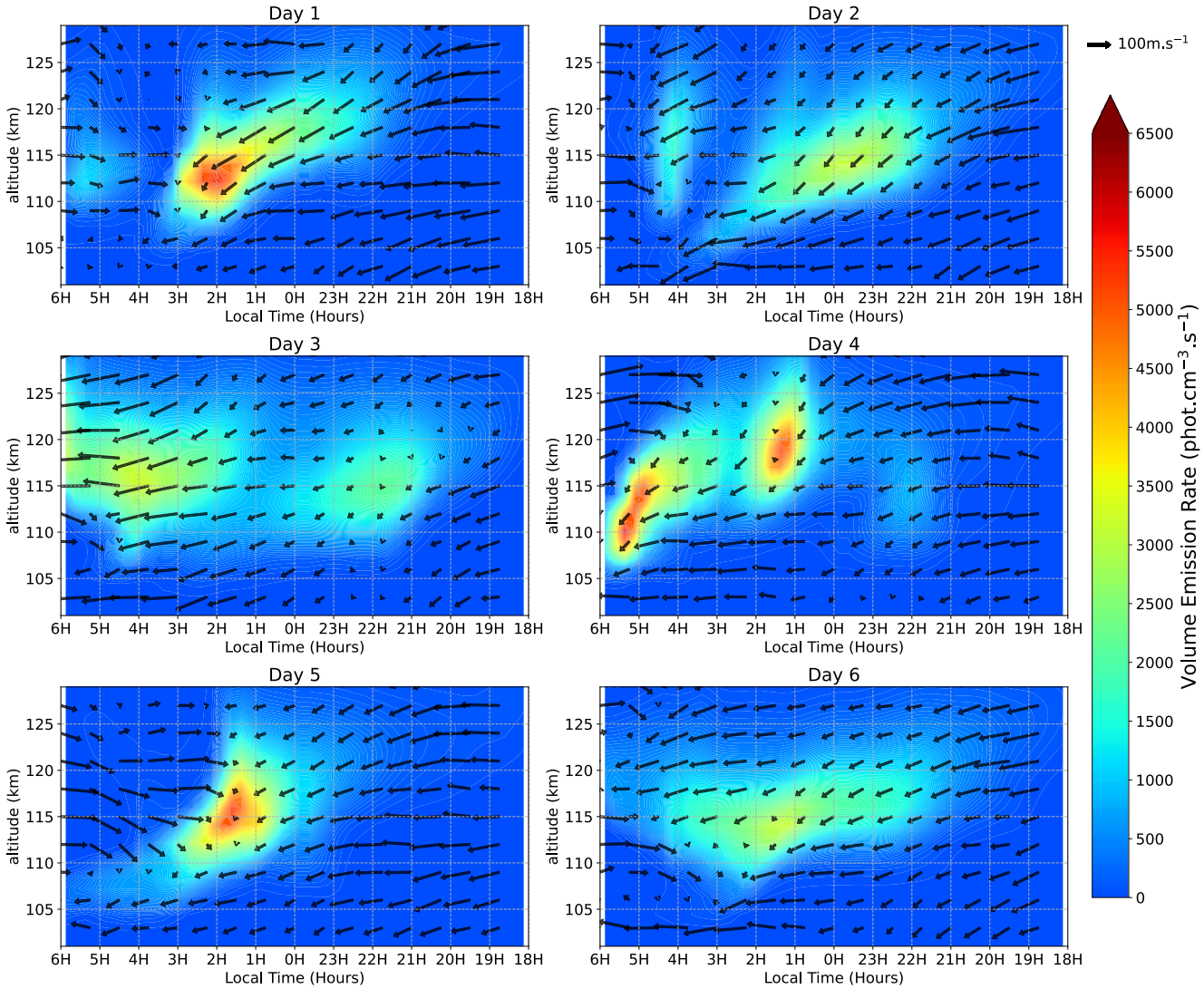

Figure 6. Vertical cross-section of the instantaneous NO nightglow (photon cm^{-3} s^{-1}) and wind (m s^{-1}) calculated in the 5°N–5°S latitude band by the Venus PCM over the six consecutive Earth days considered in Figure 4.

at the Equator and 02:00 LT, but shows a complex structure at a given time. The wind is oriented slightly more westward on average, resulting in an asymmetry of the SS-AS zonal flow between the morning and evening branches, and a shifted convergence westward of the antisolar point. As shown by previous studies using the Venus PCM, this wind asymmetry results essentially from the westward 5-day period Kelvin wave originating in the cloud deck (Navarro et al., 2021), combined with a westward acceleration of the zonal wind when non-orographic gravity waves brake in the lower thermosphere (Gilli et al., 2021). We also observe each day in Figure 5, a substantial poleward transport in both hemispheres, driven by the formation of large-scale (>1,000 km) vortices that vary on a daily timescale on the morning side. This phenomenon, which explains the presence of secondary maxima of NO nightglow at mid-to-high latitudes, is quite similar to what Navarro et al. (2021) observed for the $O_2(^1\Delta)$ emission at 1.27 μm, occurring lower at 95 km.

Examination of the NO nightglow on vertical cross-sections (Figure 6) shows a day-to-day variability comparable, if not greater, to that predicted on the horizontal plane. On the sample of six Earth days chosen here, the Mars PCM calculates an equatorial airglow that differs radically from one day to the next. On this equatorial average over 5°N–5°S, several distinct maxima can be produced during the night, and can appear as early as 22:30 LT and as late as the morning terminator at 06:00 LT. The altitude of the emission peak also varies within approximately 5 km around 115 km from one day to the next, in fairly good agreement with the SPICAV

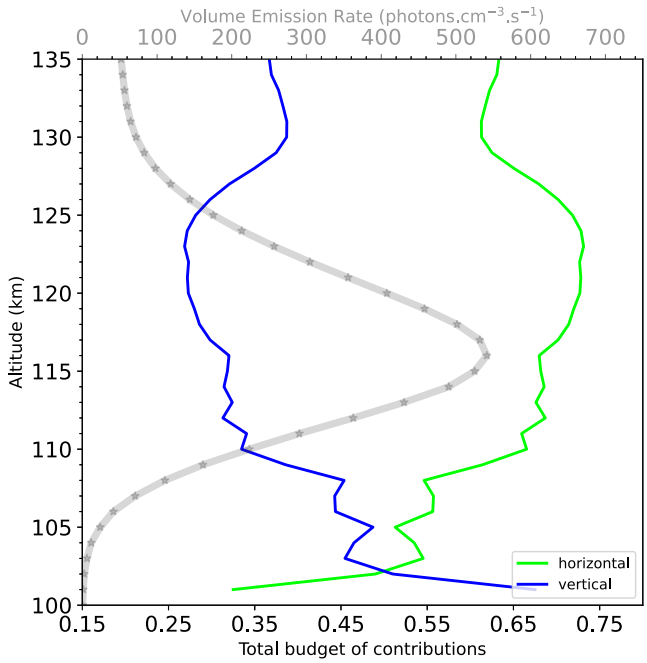

Figure 7. Relative contribution of horizontal and vertical transport to the apparent variation of NO nightglow. Data are averaged over the grid points showing more than 50 photon cm^{-3} s^{-1}. The gray curve shows the mean.

observations carried out in limb (Gérard et al., 2008; Stiepen et al., 2012) and star occultation (Royer et al., 2010, 2016) mode. The model shows no correlation between the altitude of the emission peak and the local time, as in Royer et al. (2016).

The horizontal wind convergence displayed in Figure 5 results in downward transport in Figure 6. NO emission regions are correlated with subsidence regions, and the intensity of the emission reflects that of subsidence, as in the 2D simulations of Collet et al. (2010). In Figure 6, the downward branch of the antisolar circulation is never purely vertical and generally has a strong westward component. In these areas, the N and O atoms produced by photodissociation on the dayside undergo downward transport until their number density is sufficient to initiate their recombination and produce the nightglow. This process continues during the descent until about 110 km and the complete exhaustion of N atoms, which are much less abundant than those of O (Figure 1). In subsidence zones, the vertical velocities calculated by the Venus PCM are in the range 10–20 cm s^{-1}. These values are compatible with those of 3–21 cm s^{-1} discussed by Gérard et al. (2009) to explain the shift between NO and $O_2(^1\Delta)$ emissions or the temperature enhancements in the nocturnal mesosphere (Bailey et al., 2008).

Figures 5 and 6 show that both the horizontal and the vertical transport contribute to the nightglow variability in the model. We quantified their respective contributions by decomposing the horizontal and vertical components of the advection term in the expression of the variation over time of the NO nightglow, as in Navarro et al. (2021). The result is shown in Figure 7. Generally, the effect of horizontal transport dominates that of vertical transport, but the two contributions have fairly comparable values. These results are similar to those obtained by Navarro et al. (2021) for the $O_2(^1\Delta)$ nightglow.

5. Conclusions

Our model simulations have revealed a complex, three-dimensional morphology of the NO nightglow on Venus. The contours of this emission region can extend into filaments thousands of kilometers in length across nearly all latitudes and local times. These features could not be well described by the Pioneer and Venus Express space missions due to their limited imaging capabilities. Nevertheless, the strong spatio-temporal variability that is evident in past measurements (Bougher et al., 1990; Gérard et al., 2008; Royer et al., 2010) is well reproduced by our model. It can be explained by abrupt changes, on timescales shorter than an Earth day, in the three-dimensional wind field on the nightside of Venus. In our simulations, the NO nightglow therefore never looks the same from one day to the next. Distortions of the region of NO emission are caused by the strong variations in the zonal wind and the formation of large-scale transient vortices on the horizontal plane, as in the simulations of the $O_2(^1\Delta)$ nightglow occurring 20 km lower (Navarro et al., 2021). In our simulations, the origin of these perturbations and the resulting poleward transport episodes of NO lies in the combination of the effects of the Kelvin wave and the breaking of non-orographic gravity waves in the mesosphere, as recently demonstrated with the same model by Navarro et al. (2021) and Gilli et al. (2021). We find that peak NO nightglow brightness aligns in general with maximum horizontal wind convergence, associated with a localized descent of N atom-rich air. When averaged over a long period, the modeled nightglow profile peaks at 115 km altitude. The NO bright patch is located at the equator and is shifted toward the morning terminator around 02:00 LT. This statistical result is consistent with the OUVS measurements on board Pioneer and SPICAV on board Venus Express. In quantitative terms, the mean value of NO emission calculated at 115 km is 53 kR, in excellent agreement (5%) with the value deduced from the SPICAV data set (Stiepen et al., 2012). This result suggests that the current nitrogen kinetics does not present a fundamental problem in reproducing the observed nightglow, provided that the N profile on the nightside is consistent with the Pioneer measurements.

Conflict of Interest

The authors declare no conflicts of interest relevant to this study.

Availability Statement

The SPICAV and model data presented in this study are available in this in-text data citation reference: Streel (2025).

Acknowledgments
L. Soret is supported by the Belgian national fund for scientific research (FNRS). A. Martinez is funded by Junta de Andalucia through the program EMERGIA 2021 (EMC21 00249). A. Martinez also acknowledges financial support from the Severo Ochoa grant CEX2021-001131-S funded by MCIN/AEI/10.13039/501100011033, and the Spanish Prototype of an SRC (SPSRC) service and support funded by the Ministerio de Ciencia, Innovación *y* Universidades (MICIU), by the Junta de Andalucía, by the European Regional Development Funds and by the European Union Next Generation EU/PRTR. Aurélien Stolzenbach acknowledges the support of project PID2021-126365NB-C21 funded by MCIN/AEI/10.13039/501100011033/and FEDER. N.S. was supported by the Institute for Basic Science (IBS-R035-C1). Open access publication funding provided by COUPERIN CY26.

References

Bailey, J., Meadows, V., Chamberlain, S., & Crisp, D. (2008). The temperature of the Venus mesosphere from $O_2(a^1\Delta_g)$ airglow observations. *Icarus*, *197*(1), 247–259. https://doi.org/10.1016/j.icarus.2008.04.007

Bertaux, J.-L., Nevejans, D., Korablev, O., Villard, E., Quémerais, E., Neefs, E., et al. (2007). SPICAV on Venus express: Three spectrometers to study the global structure and composition of the Venus atmosphere. *Planetary and Space Science*, *55*(12), 1673–1700. https://doi.org/10.1016/j.pss.2007.01.016

Bougher, S. W., Brecht, A. S., Schulte, R., Fischer, J., Parkinson, C. D., Mahieux, A., et al. (2015). Upper atmosphere temperature structure at the Venusian terminators: A comparison of SOIR and VTGCM results. *Planetary and Space Science*, *113–114*, 336–346. https://doi.org/10.1016/j.pss.2015.01.012

Bougher, S. W., Gérard, J. C., Stewart, A. I. F., & Fesen, C. G. (1990). The Venus nitric oxide night airglow: Model calculations based on the Venus thermospheric general circulation model. *Journal of Geophysical Research*, *95*(A5), 6271–6284. https://doi.org/10.1029/JA095iA05p06271

Brecht, A. S., Bougher, S. W., Gérard, J.-C., Parkinson, C. D., Rafkin, S., & Foster, B. (2011). Understanding the variability of nightside temperatures, NO UV and O_2 IR nightglow emissions in the Venus upper atmosphere. *Journal of Geophysical Research*, *116*(E8), E08004. https://doi.org/10.1029/2010JE003770

Collet, A., Cox, C., & Gérard, J.-C. (2010). Two-dimensional time-dependent model of the transport of minor species in the Venus night side upper atmosphere. *Planetary and Space Science*, *58*(14), 1857–1867. https://doi.org/10.1016/j.pss.2010.08.016

Crisp, D. (1986). Radiative forcing of the Venus mesosphere: I. Solar fluxes and heating rates. *Icarus*, *67*(3), 484–514. https://doi.org/10.1016/0019-1035(86)90126-0

Eymet, V., Fournier, R., Dufresne, J.-L., Lebonnois, S., Hourdin, F., & Bullock, M. A. (2009). Net exchange parameterization of thermal infrared radiative transfer in Venus' atmosphere. *Journal of Geophysical Research*, *114*(E11). https://doi.org/10.1029/2008JE003276

Feldman, P. D., Moos, H. W., Clarke, J. T., & Lane, A. L. (1979). Identification of the UV nightglow from Venus. *Nature*, *279*(5710), 221–222. https://doi.org/10.1038/279221a0

Ford, P. G., & Pettengill, G. H. (1992). Venus topography and kilometer-scale slopes. *Journal of Geophysical Research*, *97*(E8), 13103–13114. https://doi.org/10.1029/92JE01085

Fox, J. L., Galand, M. I., & Johnson, R. E. (2008). Energy deposition in planetary atmospheres by charged particles and solar photons. *Space Science Reviews*, *139*(1–4), 3–62. https://doi.org/10.1007/s11214-008-9403-7

Gérard, J.-C., Bougher, S. W., López-Valverde, M. A., Pätzold, M., Drossart, P., & Piccioni, G. (2017). Aeronomy of the Venus upper atmosphere. *Space Science Reviews*, *212*(3–4), 1617–1683. https://doi.org/10.1007/s11214-017-0422-0

Gérard, J.-C., Cox, C., Saglam, A., Bertaux, J.-L., Villard, E., & Nehmé, C. (2008). Limb observations of the ultraviolet nitric oxide nightglow with SPICAV on board Venus express. *Journal of Geophysical Research*, *113*(E5), E00B03. https://doi.org/10.1029/2008JE003078

Gérard, J.-C., Cox, C., Soret, L., Saglam, A., Piccioni, G., Bertaux, J.-L., & Drossart, P. (2009). Concurrent observations of the ultraviolet nitric oxide and infrared O_2 nightglow emissions with Venus express. *Journal of Geophysical Research*, *114*(E9). https://doi.org/10.1029/2009JE003371

Gérard, J.-C., Stewart, A. I. F., & Bougher, S. W. (1981). The altitude distribution of the Venus ultraviolet nightglow and implications on vertical transport. *Geophysical Research Letters*, *8*(6), 633–636. https://doi.org/10.1029/GL008i006p00633

Gilli, G., Lebonnois, S., González-Galindo, F., López-Valverde, M. A., Stolzenbach, A., Lefèvre, F., et al. (2017). Thermal structure of the upper atmosphere of Venus simulated by a ground-to-thermosphere GCM. *Icarus*, *281*, 55–72. https://doi.org/10.1016/j.icarus.2016.09.016

Gilli, G., Navarro, T., Lebonnois, S., Quirino, D., Silva, V., Stolzenbach, A., et al. (2021). Venus upper atmosphere revealed by a GCM: II. Model validation with temperature and density measurements. *Icarus*, *366*, 114432. https://doi.org/10.1016/j.icarus.2021.114432

Kasprzak, W. T., Niemann, H. B., Hedin, A. E., Bougher, S. W., & Hunten, D. M. (1993). Neutral composition measurements by the Pioneer Venus neutral mass spectrometer during orbiter re-entry. *Geophysical Research Letters*, *20*(23), 2747–2750. https://doi.org/10.1029/93GL02241

Krasnopolsky, V. A. (2010). Venus night airglow: Ground-based detection of OH, observations of O_2 emissions, and photochemical model. *Icarus*, *207*(1), 17–27. https://doi.org/10.1016/j.icarus.2009.10.019

Krasnopolsky, V. A. (2013). Nighttime photochemical model and night airglow on Venus. *Planetary and Space Science*, *85*, 78–88. https://doi.org/10.1016/j.pss.2013.05.022

Lebonnois, S., Hourdin, F., Eymet, V., Crespin, A., Fournier, R., & Forget, F. (2010). Superrotation of Venus' atmosphere analyzed with a full general circulation model. *Journal of Geophysical Research*, *115*(E6). https://doi.org/10.1029/2009JE003458

Lefèvre, F., Trokhimovskiy, A., Fedorova, A., Baggio, L., Lacombe, G., Määttänen, A., et al. (2021). Relationship between the ozone and water vapor columns on Mars as observed by SPICAM and calculated by a global climate model. *Journal of Geophysical Research: Planets*, *126*(4), e2021JE006838. https://doi.org/10.1029/2021JE006838

Martinez, A., Chaufray, J.-Y., Lebonnois, S., Gonzàlez-Galindo, F., Lefèvre, F., & Gilli, G. (2024). Three-dimensional Venusian ionosphere model. *Icarus*, *415*, 116035. https://doi.org/10.1016/j.icarus.2024.116035

Martinez, A., Lebonnois, S., Millour, E., Pierron, T., Moisan, E., Gilli, G., & Lefèvre, F. (2023). Exploring the variability of the venusian thermosphere with the IPSL Venus GCM. *Icarus*, *389*, 115272. https://doi.org/10.1016/j.icarus.2022.115272

Navarro, T., Gilli, G., Schubert, G., Lebonnois, S., Lefèvre, F., & Quirino, D. (2021). Venus' upper atmosphere revealed by a GCM: I. Structure and variability of the circulation. *Icarus*, *366*, 114400. https://doi.org/10.1016/j.icarus.2021.114400

Niemann, H. B., Booth, J. R., Cooley, J. E., Hartle, R. E., Kasprzak, W. T., Spencer, N. W., et al. (1980). Pioneer Venus orbiter neutral gas mass spectrometer experiment. *IEEE Transactions on Geoscience and Remote Sensing, GE-*, *18*(1), 60–65. https://doi.org/10.1109/TGRS.1980.350282

Royer, E., Montmessin, F., & Bertaux, J.-L. (2010). NO emissions as observed by SPICAV during stellar occultations. *Planetary and Space Science*, *58*(10), 1314–1326. https://doi.org/10.1016/j.pss.2010.05.015

Royer, E., Montmessin, F., & Marcq, E. (2016). Variability of the nitric oxide nightglow at Venus during solar minimum. *Journal of Geophysical Research: Planets*, *121*(5), 846–853. https://doi.org/10.1002/2016JE005013

Soret, L., Gérard, J.-C., Montmessin, F., Piccioni, G., Drossart, P., & Bertaux, J.-L. (2012). Atomic oxygen on the Venus nightside: Global distribution deduced from airglow mapping. *Icarus*, *217*(2), 849–855. https://doi.org/10.1016/j.icarus.2011.03.034

Soret, L., Gérard, J.-C., Piccioni, G., & Drossart, P. (2014). Time variations of $O_2(a^1\Delta)$ nightglow spots on the Venus nightside and dynamics of the upper mesosphere. *Icarus*, *237*, 306–314. https://doi.org/10.1016/j.icarus.2014.03.034

Stewart, A. I., & Barth, C. A. (1979). Ultraviolet night airglow of Venus. *Science*, *205*(4401), 59–62. https://doi.org/10.1126/science.205.4401.59

Stewart, A. I., Gérard, J.-C., Rusch, D. W., & Bougher, S. W. (1980). Morphology of the Venus ultraviolet night airglow. *Journal of Geophysical Research*, *85*(A13), 7861–7870. https://doi.org/10.1029/JA085iA13p07861

Stiepen, A., Gérard, J.-C., Dumont, M., Cox, C., & Bertaux, J.-L. (2013). Venus nitric oxide nightglow mapping from SPICAV nadir observations. *Icarus*, *226*(1), 428–436. https://doi.org/10.1016/j.icarus.2013.05.031

Stiepen, A., Soret, L., Gérard, J.-C., Cox, C., & Bertaux, J.-L. (2012). The vertical distribution of the Venus NO nightglow: Limb profiles inversion and one-dimensional modeling. *Icarus*, *220*(2), 981–989. https://doi.org/10.1016/j.icarus.2012.06.029

Stolzenbach, A., Lefèvre, F., Lebonnois, S., & Määttänen, A. (2023). Three-dimensional modeling of Venus photochemistry and clouds. *Icarus*, *395*, 115447. https://doi.org/10.1016/j.icarus.2023.115447

Streel, N. (2025). Dataset in support of paper "Strong variability of the modeled Venus NO nightglow" [Dataset]. *Zenodo*. https://doi.org/10.5281/ZENODO.15848151

Von Zahn, U., Fricke, K. H., Hunten, D. M., Krankowsky, D., Mauersberger, K., & Nier, A. O. (1980). The upper atmosphere of Venus during morning conditions. *Journal of Geophysical Research*, *85*(A13), 7829–7840. https://doi.org/10.1029/JA085iA13p07829

References From the Supporting Information

Adams, N. G., Smith, D., & Paulson, J. F. (1980). An experimental survey of the reactions of NHn^+ ions (n = 0 to 4) with several diatomic and polyatomic molecules at 300 K. *The Journal of Chemical Physics*, *72*(1), 288–297. https://doi.org/10.1063/1.438893

Allen, M., & Frederick, J. E. (1982). Effective photodissociation cross sections for molecular oxygen and nitric oxide in the schumann-runge bands. *Journal of the Atmospheric Sciences*, *39*(9), 2066–2075. https://doi.org/10.1175/1520-0469(1982)039<2066:EPCSFM>2.0.CO;2

Anicich, V. G. (1993). Evaluated bimolecular ion-molecule gas phase kinetics of positive ions for use in modeling planetary atmospheres, cometary Comae, and interstellar clouds. *Journal of Physical and Chemical Reference Data*, *22*(6), 1469–1569. https://doi.org/10.1063/1.555940

Atkinson, R., Baulch, D. L., Cox, R. A., Hampson, R. F., Kerr (Chairman), J. A., & Troe, J. (1989). Evaluated kinetic and photochemical data for atmospheric chemistry: Supplement III. IUPAC subcommittee on gas kinetic data evaluation for atmospheric chemistry. *Journal of Physical and Chemical Reference Data*, *18*(2), 881–1097. https://doi.org/10.1063/1.555832

Brune, W. H., Schwab, J. J., & Anderson, J. G. (1983). Laser magnetic resonance, resonance fluorescence, and resonance absorption studies of the reaction kinetics of $O + OH \rightarrow H + O_2$, $O + HO_2 \rightarrow OH + O_2$, $N + OH \rightarrow H + NO$, and $N + HO_2 \rightarrow$ products at 300 K between 1 and 5 torr. *The Journal of Physical Chemistry*, *87*(22), 4503–4514. https://doi.org/10.1021/j100245a034

Burkholder, J. B., Sander, S. P., Abbatt, J. P. D., Barker, J. R., Cappa, C., Crounse, J. D., et al. (2020). Chemical kinetics and photochemical data for use in atmospheric studies. *Evaluation Number*, *19*, 1610.

Chan, W. F., Cooper, G., Sodhi, R. N. S., & Brion, C. E. (1993). Absolute optical oscillator strengths for discrete and continuum photoabsorption of molecular nitrogen (11–200 eV). *Chemical Physics*, *170*(1), 81–97. https://doi.org/10.1016/0301-0104(93)80095-Q

Copp, N. W., Hamdan, M., Jones, J. D. C., Birkinshaw, K., & Twiddy, N. D. (1982). A selected ion flow tube study of the reactions of the gaseous ion CO^+_2 at 298 K. *Chemical Physics Letters*, *88*(5), 508–511. https://doi.org/10.1016/0009-2614(82)83164-3

Du, M. L., & Dalgarno, A. (1990). The radiative association of N and O atoms. *Journal of Geophysical Research*, *95*(A8), 12265–12268. https://doi.org/10.1029/JA095iA08p12265

Fox, J. L., & Sung, K. Y. (2001). Solar activity variations of the Venus thermosphere/ionosphere. *Journal of Geophysical Research*, *106*(A10), 21305–21335. https://doi.org/10.1029/2001JA000069

Herron, J. T. (1999). Evaluated chemical kinetics data for reactions of $N(^2D)$, $N(^2P)$, and $N_2(A\ 3\Sigma u+)$ in the gas phase. *Journal of Physical and Chemical Reference Data*, *28*(5), 1453–1483. https://doi.org/10.1063/1.556043

Jenouvrier, A., Coquart, B., & Merienne, M. F. (1996). The NO_2 absorption spectrum. III: The 200–300 nm region at ambient temperature. *Journal of Atmospheric Chemistry*, *25*(1), 21–32. https://doi.org/10.1007/BF00053284

Jones, J. D. C., Birkinshaw, K., & Twiddy, N. D. (1981). Rate coefficients and product ion distributions for the reactions of OH^+ and H_2O^+ with N_2 , O_2, NO. N_2O, Xe, CO, CO_2, H_2S and H_2 at 300 K. *Chemical Physics Letters*, *77*(3), 484–488. https://doi.org/10.1016/0009-2614(81)85191-3

Peterson, J. R., Le Padellec, A., Danared, H., Dunn, G. H., Larsson, M., Larson, A., et al. (1998). Dissociative recombination and excitation of N_2^+: Cross sections and product branching ratios. *The Journal of Chemical Physics*, *108*(5), 1978–1988. https://doi.org/10.1063/1.475577

Campbell, I. M., & Thrush, B. A. (1966). Behaviour of carbon dioxide and nitrous oxide in active nitrogen. *Transactions of the Faraday Society*, *62*, 3366–3374. https://doi.org/10.1039/TF9666203366

Rakshit, A. B., & Warneck, P. (1980). Reactions of CO_2^+, $CO_2CO_2^+$ and H_2O^+ ions with various neutral molecules. *Journal of the Chemical Society, Faraday Transactions 2: Molecular and Chemical Physics*, *76*, 1084–1092. https://doi.org/10.1039/F29807601084

Schunk, R. W., & Nagy, A. F. (2000). *Ionospheres: Physics, plasma physics, and chemistry*. Cambridge University Press.

Vandaele, A. C., Hermans, C., Simon, P. C., Carleer, M., Colin, R., Fally, S., et al. (1998). Measurements of the NO_2 absorption cross-section from 42 000 cm^{-1} to 10 000 cm^{-1} (238–1000 nm) at 220 K and 294 K. *Journal of Quantitative Spectroscopy and Radiative Transfer*, *59*(3), 171–184. https://doi.org/10.1016/S0022-4073(97)00168-4